2016-32-0033
20168033
Published 11/08/2016

doi:10.4271/2016-32-0033
saeeng.saejournals.org

Measurement and Prediction of Heat Transfer Losses on the XMv3 Rotary Engine

Tiago J. Costa
Universidade do Minho

Mark Nickerson and Daniele Littera
LiquidPiston Inc

Jorge Martins
Universidade do Minho

Alexander Shkolnik and Nikolay Shkolnik
LiquidPiston Inc

Francisco Brito
Universidade do Minho

ABSTRACT

This paper describes predictive models and validation experiments used to quantify the in-chamber heat transfer of LiquidPiston's rotary 70cc SI "XMv3" engine.

The XMv3 engine is air cooled, with separate cooling flow paths for the stationary parts and the rotor. The heat transfer rate to the stationary parts was measured by thermal energy balance of that circuit's cooling air. However, because the rotor's cooling air mixes internally with the engine's exhaust gas, a similar procedure was not practical for the rotor circuit. Instead, a CONVERGE CFD model was developed, and used together with GT-POWER to derive boundary conditions to estimate a ratio between rotor and stationary parts heat transfer, thus allowing estimation of rotor and total heat losses.

For both cases studied (5000 and 9000 rpm under full load), the rotor's heat loss was found to be ~60% that of the stationary parts, and overall heat losses were less than 35% of supplied fuel energy.

The significance of this work relates to the following facts:

- It represents the first time that heat transfer was quantified for the "X" engine architecture;
- Preliminary experimental and modelling results show reasonable correlation
- The predictive models developed will inform future engine cooling system optimization work, leading to higher power densities and thermal efficiencies. Results for these two metrics are already market competitive in the 3 horsepower engine size.

CITATION: Costa, T., Nickerson, M., Littera, D., Martins, J. et al., "Measurement and Prediction of Heat Transfer Losses on the XMv3 Rotary Engine," *SAE Int. J. Engines* 9(4):2016, doi:10.4271/2016-32-0033.

INTRODUCTION

Heat loss from the working fluid to the combustion chamber is an important driver for engine performance, durability, fuel economy, and exhaust emissions. For a given mass of fuel within the chamber, higher heat transfer to the walls lowers the average gas temperature and pressure, and therefore reduces the work produced per cycle. As engine size decreases, the energy fraction lost through heat transfer tends to increase due to the associated increase in surface area to volume ratio. Engine architecture also plays a big rule on this ratio, with rotary engines having a higher ratio than conventional piston engines for the same chamber displacement [1], [2]. Overall, the amount of heat transferred to the engine walls is predominantly affected by the surface to volume ratio at Top Dead Center (TDC),

charge motion and flame quenching distance (both affecting the heat transfer coefficient), the difference between gas and wall temperature, and the time available for heat transfer to occur (engine speed).

LiquidPiston's "X" architecture is a rotary engine embodiment similar in some aspects to the Wankel. A significant benefit of the "X" engine architecture is the ability to more closely follow LiquidPiston's optimized 4-stroke cycle, dubbed the High Efficiency Hybrid Cycle (HEHC) [3], which incorporates both constant volume combustion and over-expansion [4], [5]. The surface area to volume ratio (SA/V) of the combustion chamber is lower for "X" architecture, compared to piston engines of similar displacement and performance. However, at the beginning of the expansion stroke, the combustion chamber opens into a larger area that has rather larger SA/V than piston engines. It is, therefore, important to quantify real-life heat transfer losses, and also to develop predictive models for this purpose.

The XMv3 (at 70cc total displacement) is LiquidPiston's smallest "X" engine prototype, and it is cooled by a crankshaft mounted centrifugal fan. The design of the cooling circuit separates airflow paths for 1) all stationary parts (main housing, side covers, etc.), and 2) the rotor (also the most challenging component to cool). Heat transfer through the stationary parts was measured experimentally by a standard thermal energy balance technique. However, a similar procedure was not possible for the rotor circuit, as the exiting cooling air is mixed with engine exhaust flow before those temperatures can be separately measured. Instead, a CONVERGE CFD model was used to derive a ratio between "rotor" and "stationary parts" heat losses, and the ratio then used to estimate rotor and total heat losses during the experiments.

Following a literature review, an overview of the tested XMv3 engine will be presented, focusing on its unique gas flow paths. LPI's experimental methods, GT-POWER 1D, and CONVERGE CFD models are next described. Finally, the calculation procedure used to derive net heat transfer losses is presented. The paper is concluded with a discussion of anticipated future work.

Piston/Wankel Engine Heat Transfer Modeling Methods

For piston engines, empirical correlations have been formulated to predict in-chamber heat transfer losses as functions of engine operating conditions [6]. These models typically calculate instantaneous convective heat transfer coefficients through simplified empirical correlations for flow over flat plates or in pipes. The most widely used piston engine correlation was published by Woschni in 1967 [7]. A heat transfer correlation based on turbulent Couette flow was developed to better predict heat transfer losses in Wankel rotary engines [8]. This model was able to differentiate between the rotor and housing heat transfer coefficients. However, in general, these models are not used to describe the details of local or unsteady heat transfer effects, and must be calibrated using experimental results for different engine types. Once all coefficients are tuned, a completed "0D/1D" model can be used to explain or roughly predict overall engine performance such as power output, fuel consumption, total heat loss, exhaust temperature, etc. These types of models are most often used in the early stages of engine design, due to their simplicity, albeit at limited accuracy.

Heat transfer in real combustion engines is known to be an unsteady and three-dimensional phenomenon. More recently, thanks to advances in computing, CFD numerical codes have become increasingly valuable tools for performing accurate heat transfer simulations [6]. These models have the advantage of being able to provide more detailed information about the local in-cylinder flow pattern and behavior, at the expense of added complexity and time. A CFD model requires a CAD geometry and an accurate understanding of boundary conditions for fuel, intake air, exhaust, etc., so they are typically used later in the engine design process.

Another challenge in CFD modeling is choosing appropriate sub-models, for example, one to describe near wall heat transfer. An extensive CFD code investigation was performed by Rakopoulos [9], where different wall heat transfer models were compared with experimental heat flux measurements from spark ignition and diesel engines. For the calculation of the wall heat fluxes, an in-house CFD model was validated against numerical results obtained using wall-function formulations, such as those of Han [10], and Huh. Han's model, although having a very simple formulation, consistently captured the magnitude of peak heat flux and its trend during the compression and expansion strokes.

It is of the utmost importance to experimentally measure the heat transfer to the engine components in order to validate the empirical or computational models. This measurement is typically performed by an energy balance analysis as the engine is run under controlled conditions. It is also possible to directly measure heat flux to the combustion chamber walls, but this technique requires the adoption of complex, expensive, and intrusive sensors [11], which in some cases cannot be easily used, for example, to measure the heat flux on moving parts such as a piston or the rotor of a Wankel engine [12].

Wankel Experimental Heat Transfer Results

Due to the similarities between the "X" and the Wankel engine architectures, it is helpful to review some research on Wankel engine cooling losses, with focus on experimental data.

One of the most complete sets of experimental thermal balance data was published by Badgley [13]. A stratified JP-8 charge, 160 horsepower, turbocharged Wankel engine was tested at 8000 RPM. Extensive energy related measurements were taken, allowing the calculation of heat losses with two different methods. The final error between methods was 3% of the fuel energy. These results are relevant because the Wankel engine, has a relatively larger SA/V ratio than a conventional piston engine, which is also true during expansion stroke of "X" engines, so intuitively could suffer from higher heat transfer losses. This was not the case, however, with just 12% of fuel energy in this experiment being rejected to the cooling and oil systems. A typical value for a piston engine would be 20-36% [14].The reasons for such low heat loss were not discussed in the

work, but there are three likely hypotheses. These are: the unusually low compression ratio (7.5:1), the stratified charge fueling strategy, and relatively high engine speed.

Another report from NASA [15], showed test results of a Mazda 12B spark ignition engine (2 rotor, carbureted, with a 9.4:1 compression ratio, and a total displacement per rotor of 573cc). The results showed a maximum cooling loss of 20% at 4500 rpm.

An important takeaway from these investigations is that rotary engines are capable, under the right circumstances, of quite low heat transfer losses. In fact, no engineering literature was found to report the intuitively expected high Wankel heat losses. With this in mind, it is pertinent to perform a comparison between the "X" and the Wankel engines, in order to understand if similar results might be expected for LiquidPiston's engine.

ENGINE OVERVIEW

The prototype engine investigated in this work, XMv3, is a spark ignition (SI), four-stroke variant of the "X" architecture, and its development is ongoing. It has a single rotor, three combustion chambers, an overall displacement of 70cc (23 cc per chamber), and produces 3hp at 10,000 rpm. A detailed description of prior XMv3 engine developments can be found in papers [16], [17].

For an animation describing the operation of the XMv3 engine, please visit: http://liquidpiston.com/technology/x-mini-gasoline/.

Table 1 lists basic XMv3 engine parameters. Worthy of note is the compression ratio vs. expansion ratio, the difference intentionally designed to provide an adjustable degree of over-expansion by asymmetrical location of the intake and exhaust ports in the rotor. This asymmetry is also seen in the port timing numbers. While the XMv3 configuration as tested had a limited over-expansion ratio of 1.12, some of LiquidPiston's other prototype engines, designed for higher efficiency operation on diesel, have significantly higher over-expansion ratios in excess of 1.5.

Table 1. Tested XMv3 engine specifications.

Number of rotors	1
Overall displacement (cc)	69
Displacement per chamber (cc)	23
Nominal compression ratio (CR)	9.26:1
Effective CR	8.07:1
Effective expansion ratio	9.05:1
Over expansion ratio (Effective expansion ratio/ Effective CR)	1.12
Intake valve closing (ºCA BTDC)	135
Exhaust valve opening (ºCA ATDC)	161

Comparison to Wankel

In many ways, the "X" engine can be thought of as an inverted Wankel. The rotor in both engine types is mounted on an eccentric shaft, so that its center moves on a circle, with the rotor being turned by a gear. In the case of the Wankel, however, the small gear is fixed to the stationary housing, while in the "X" engine the small gear is fixed to the moving rotor. As can be seen in Figure 1, the "X" engine rotor has the same epitrochoid shape as the Wankel housing. These parts are both divided into two symmetric lobes, one seeing mainly intake/exhaust strokes, and the other compression and expansion strokes (the "hot side"). The Wankel has a three lobed rotor, with each of the lobes defining a combustion chamber, similar to the housing of the "X" engine.

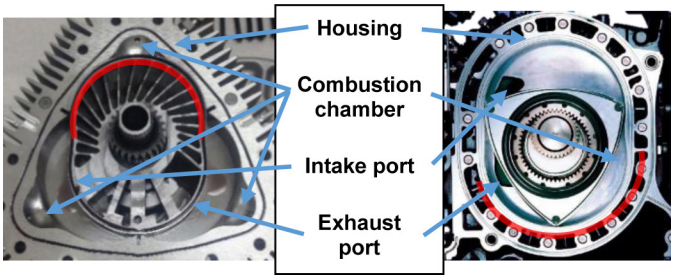

Figure 1. Comparison between the Wankel engine (right), and the "X" engine (left). The hot region of each engine is marked with a red arc.

The "X" engine has three chambers, delineated by the rotor, housing and two cover plates, and sealed by the rotor face seals and three stationary apex seals. The Wankel's three moving chambers are sealed to the side covers similarly by rotor face seals, and separated by rotor mounted (moving) apex seals. The Wankel "hot part" is the housing section that only sees combustion/expansion and exhaust strokes. Whereas the Wankel engine executes the 4-stroke cycle while moving the charge over different parts of the engine, the X engine executes the three 4-stroke cycles simultaneously in three independent combustion chambers.

The Wankel engine intake and exhaust ports are either located "peripherally" in the main housing, or "side mounted" in the side plates. The "X" engine ports, when configured as a 4-stroke, are located peripherally in the rotor.

As a result of the aforementioned porting and architecture differences, there is a significant difference between the gas flow in the combustion chamber of each engine, as shown in Figure 2. In the Wankel, gas travels with the rotor as it sweeps across the stationary housing surface, similarly to Couette flow, described as a parallel-plate flow developed by fixing one plate and moving the other one with constant velocity [18]. The "X" engine flow, on the other hand, is more similar to that of a piston engine, with the rotor rotating (relatively slowly) at the same time as translating (relatively quickly) towards or away from the housing profile, similarly to a piston moving relative to a cylinder head. The Wankel combustion chamber geometry is defined by the rotor surface geometry (like bowl-in-piston), whereas the "X" engine combustion chambers are defined by the housing, thus allowing more freedom for the X engine chamber design.

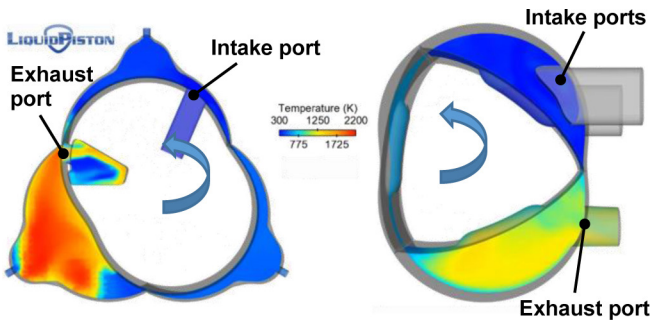

Figure 2. Fluid motion comparison between the "X" engine (left) and the Wankel engine (right).

Another important factor to compare between the two engines is the relative rotational speed of the rotor and crankshaft. The Wankel rotor runs at 1/3 shaft RPM, whereas the "X" engine ratio is 1/2. By having relatively higher rotational speed for a given airflow rate and engine size, the "X" rotor will have higher tangential velocities, possibly leading to higher fluid shear stress near the rotor walls. This could tend to increase local heat transfer coefficients if comparing at the same shaft RPM.

In conclusion, while both engines belong to the same geometrical family of rotary engines, there are significant differences in internal gas flow. These differences will ultimately affect the amount of energy that each architecture loses to heat transfer. Therefore, experimental measurement and development of a new model is necessary to best inform future work, rather than attempting to adapt existing design procedures from Wankel or piston engines to the "X" architecture.

XMv3 Gas Flow Paths

The XMv3 intake, exhaust, and cooling paths are significantly different from those of conventional piston/Wankel engines. Figure 3 shows section and front views of the XMv3, with arrows indicating the direction and position of the different flows.

Intake air (green) enters the engine through a bellmouth, where a fuel injector (not shown) is placed along the same axis as the crankshaft. The premixed charge then proceeds through a hollow crankshaft and turns 90 degrees, passing through holes drilled radially through the shaft. These holes open to a channel in the rotor, and then to the intake port, where the charge enters the working chamber.

During the exhaust stroke, combustion products (marked with red arrows) exit the active chamber via the rotor exhaust port, entering the interior volume of the rotor, therefore mixing with the rotor cooling air (blue arrows). Fan forced rotor cooling air continually passes through the engine via three matching triangular ports (red outlines) in each of the engine's side plates.

The engine's stationary elements are also air cooled, this circuit defined by plastic shrouds covering the exterior of the engine (Figure 4). The shroud's insides are fitted with air distribution vanes. Note that for these heat transfer experiments, the shaft mounted cooling fan was replaced with an external blower, allowing for more convenient measurement and control of each flow rate and temperature.

The exiting cooling air, and in the rotor circuit case, also the mixed exhaust gases, leave the engine shrouds through three segregated openings each, shown again in Figure 4

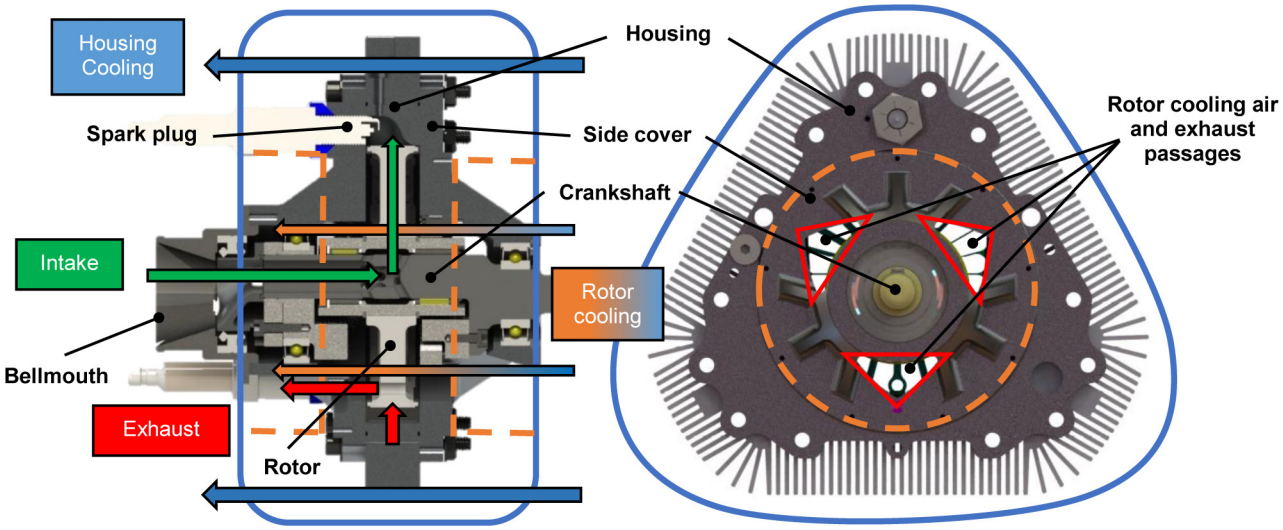

Figure 3. XMv3 engine gas path flows. Green is the intake charge, red is the exhaust, and blue is the cooling flow. The blue outlines represent the outer engine shroud, which separates the "stationary part" and "rotor cooling" flow paths at the orange dashed lines. Shown in red, three triangular openings on each side of the engine allow the passage of rotor cooling air and exhaust flows.

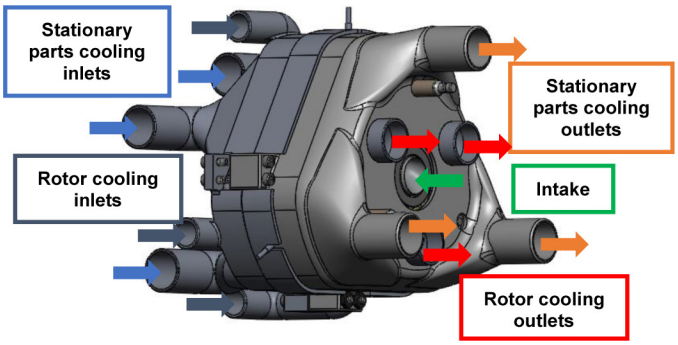

Figure 4. XMv3 engine shrouds with inlet and outlet gas flows.

EXPERIMENTAL METHODOLOGY

Engine experiments were conducted at LiquidPiston's dynamometer test facility (Figure 5). The engine was controlled by a National Instruments system capable of actuating start-of-injection timing, injection duration, and fuel pressure. The system also recorded both high speed data (crank angle resolved signals such as chamber pressures, instantaneous engine torque) and low speed data (time-based signals such as thermocouple temperatures, static pressures, etc.). The dynamic pressure signals were measured with Kistler 6052C piezoelectric transducers. Commercially available, ethanol free gasoline with a minimum octane rating of 92 (R+M)/2 was used. The fuel was premixed 50:1 with synthetic oil for lubrication of all engine bearings and seals.

Two operating conditions were studied, both full load, at 5000 and 9000 rpm. Table 2 lists key parameters for each case.

Table 2. Test engine conditions for the two cases studied.

Test case	1	2
Engine speed (RPM)	9000	5000
Intake pressure (bar)	1.03	1.01
Lambda	0.85	0.85
Spark advance (SA) (ºCA BTDC)	30	30
Cooling Air Flow to Housing / Rotor (kg/sec)	165/171	90/97

Cooling Methods and Heat Transfer Measurement/ Calculation

Cooling air for test purposes was provided by a separate motor driven blower, allowing easier control and measurement than with the usual crankshaft mounted fan.

A diverter valve was used to feed inlet air separately to the "rotor" and "stationary parts" circuits as previously described. For the stationary parts, mass flow rate (before) and air temperature (before and after) the engine were measured. This enabled calculation of the thermal energy lost to the stationary parts by thermal energy balance. A similar procedure was not possible for the rotor cooling circuit.

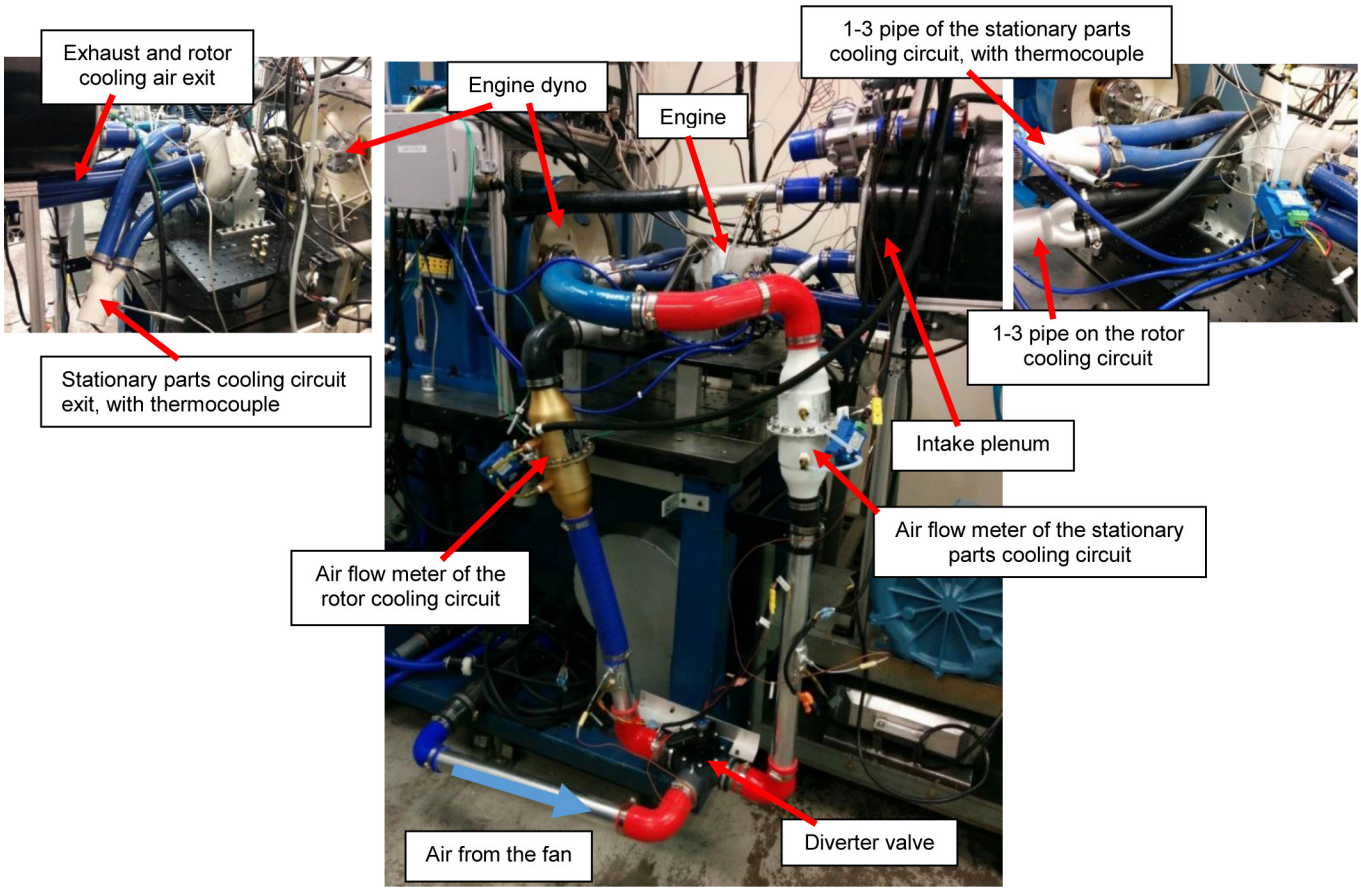

Figure 5. Overview of the engine dyno setup.

As illustrated in Figure 6, the exhaust gases exit the combustion chamber through the exhaust port, and immediately mix with the rotor cooling air before leaving the inner rotor volume. Thus, cooling air exit temperature could not be measured separately from the exhaust gas temperature.

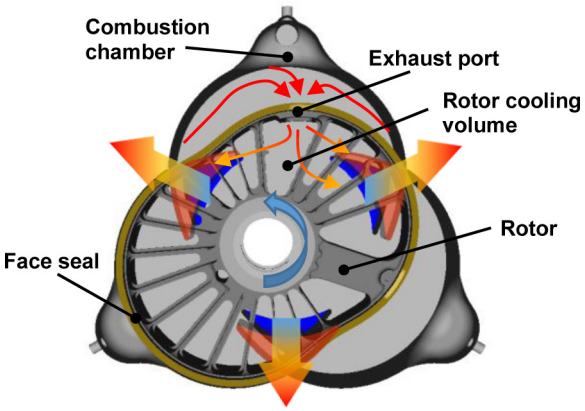

Figure 6. Exhaust gas and rotor cooling air flow inside the engine.

During these experiments, the engine was run in "cold steady state" condition by adjusting cooling flow rates. Additional data with more typical lower cooling flows is also presented, though is not matched by the CFD model. K-type thermocouples where placed in each component facing the combustion chamber gases. These included one through the housing at a central combustion chamber position, and two more on intake and exhaust side covers near the center of the chamber. Figure 7 shows the location of the thermocouples, in addition to the placements of the Kistler pressure transducer and spark plug.

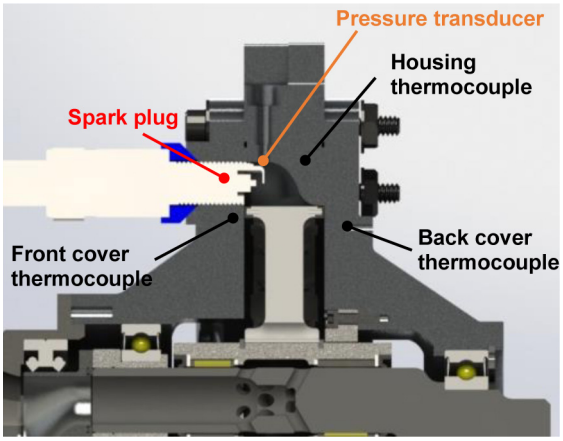

Figure 7. XMv3 section view with pressure transducer and thermocouples position.

Due to the difficulties involved in directly measuring rotor surface temperature, a K type thermocouple with 0.23 mm diameter tip was placed inside one of the engine's stationary apex seals (Figure 8). The close proximity of this thermocouple to the rotor surface (1.5 mm) was thought to give the best reasonable indication of average rotor surface temperature.

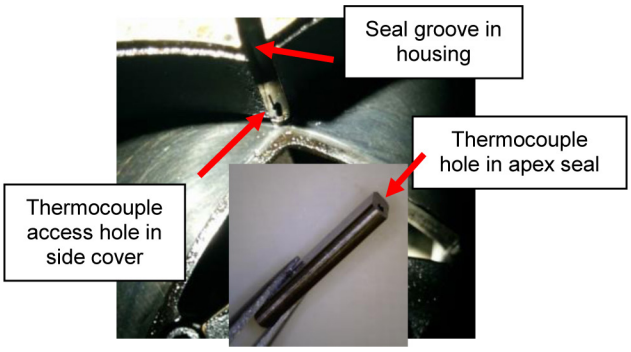

Figure 8. Apex seal thermocouple details.

Table 3 shows steady state temperature measurements from the two tested conditions. As expected, the apex seal temperature (representing the rotor surface) was highest. The front plate runs hotter than the back plate due to its larger surface area exposed to combustion gases (the quiescent chamber is facing the front plate), and also because it is exposed to less (and by then warmer) cooling air.

Table 3. Steady state temperatures for each test case.

Test case	1	2
Housing temperature (K)	470	477
Apex seal temperature (K)	518	500
Front plate temperature (K)	480	483
Back plate temperature (K)	460	468

COMPUTATIONAL METHODS

3D CFD and 1D engine modeling softwares were used for the analyses of test data and also as predictive tools.

1D Engine Modelling by GT-POWER

1D models are useful development tools because they provide insights to engine performance. They are also helpful when coupled with more advanced CFD models, for which they often provide boundary conditions not otherwise available from experimental data.

A 1D model of the XMv3 rotary engine was developed using Gamma Technology's GT-POWER. As GT-POWER was primarily designed to model piston-cylinder designs, the rotary engine was implemented using piston and cylinder approximations for each chamber via custom functions. A top-level overview of the model is seen in Figure 9. The model begins in the green box (intake components) and ends with the exhaust to the shrouds (orange boxed). Intake and exhaust tracts are modeled exactly as the experimental setup, with each smaller box representing components in each system. GEM3D was used to 1-dimensionally discretize the rotor and other complex geometry parts. The working chambers of the engine were modelled as crank-less pistons and cylinders, and a piston position array was used to account for variations of the true rotary volume profile versus that of crank-slider kinematics. A customized process was also developed to modify GT-POWER's internal heat transfer correlation (Woschni) for the XMv3, and a surface area correction factor was generated.

Test data was used to calibrate and validate the GT-POWER model. Parameters adjusted during calibration include heat transfer constants, equivalent critical flow orifice sizes for "atmospheric" leak area (modeling blow-by across the face seal) and "inter-chamber" leak area (modeling blow-by to adjacent chambers, presumably across the apex seals). Experimental heat release was matched using single or multiple Wiebe functions. The calibrated model offers insight into the engine's operation, clearly identifying where mass and energy flow within the system. The GT-POWER model is also a useful predictive and optimization tool, and perhaps most importantly, can provide time saving boundary conditions to CFD, such as mass flow rates and gas temperatures for intake, exhaust, and leakage flows.

Engine Modelling by Computational Fluid Dynamics

The three-dimensional combustion simulation software CONVERGE (developed by Convergent Science Inc.) was used to predict the heat transfer losses through the various combustion chamber walls. This powerful tool allows for automatic meshing of moving boundaries and disconnecting sections, a crucial feature to enable the modeling of a complete cycle of the XMv3 rotary engine's operation. A detailed chemistry combustion model (SAGE) was used to calculate flame front propagation and flame quenching at the engine walls, relevant for predictive heat transfer modelling. The Reynolds Averaged Navier-Stokes (RANS) based RNG k-ε model [19] was used for turbulence modelling, as recommended by CONVERGE, and it has relatively low computational power requirements. A finite volume, second-order accurate spatial scheme was used to solve all transport and momentum equations. Time step determination was handled dynamically by the code with a set range between 1.0e-05 to 1.0e-08 seconds. The time step was calculated for each cycle based on Courant-Friedrichs-Lewy (CFL) numbers. For both the convective and diffusive CFL numbers, 2 was used during the simulations. For the speed of sound, CFL equal to 50 was used.

In previous studies [17], mass flow rate, temperature, and pressure boundary conditions were applied to the inlet of the charge intake pipe and to the intake of the rotor cooling windows. In the simplified model presently described, different boundary conditions were available and taken from GT-POWER. As a result, the CFD model was simplified, with upstream intake and blow-by leak paths completely removed, enabling an enormous reduction in computational cost.

As an example, using 16 cores the run time of a multi-cycle firing simulation was reduced from 7 days to 12 hours.

Surface Preparation

In order to simulate the face, apex, and shaft seals of the XMv3 engine, CONVERGE's unique sealing capability was used. This functionality was essential to capture the rotating and translating behavior of the face seals. Three "apex" seals were used to separate working chambers, just as in the physical engine. Each was directed towards the rotor surface, preventing all gas flow leakage. Therefore, separate methods to model inter-chamber and atmospheric blow-by leaks were added. Side seals were placed along each side of the combustion chamber/housing profile and directed towards the intake and exhaust side plates.

Other upstream seals were located between fluid path transitions, where moving and stationary parts must be connected (i.e. intake pipe to bellmouth), and when the relative motion between parts is different (i.e. crankshaft to rotor).

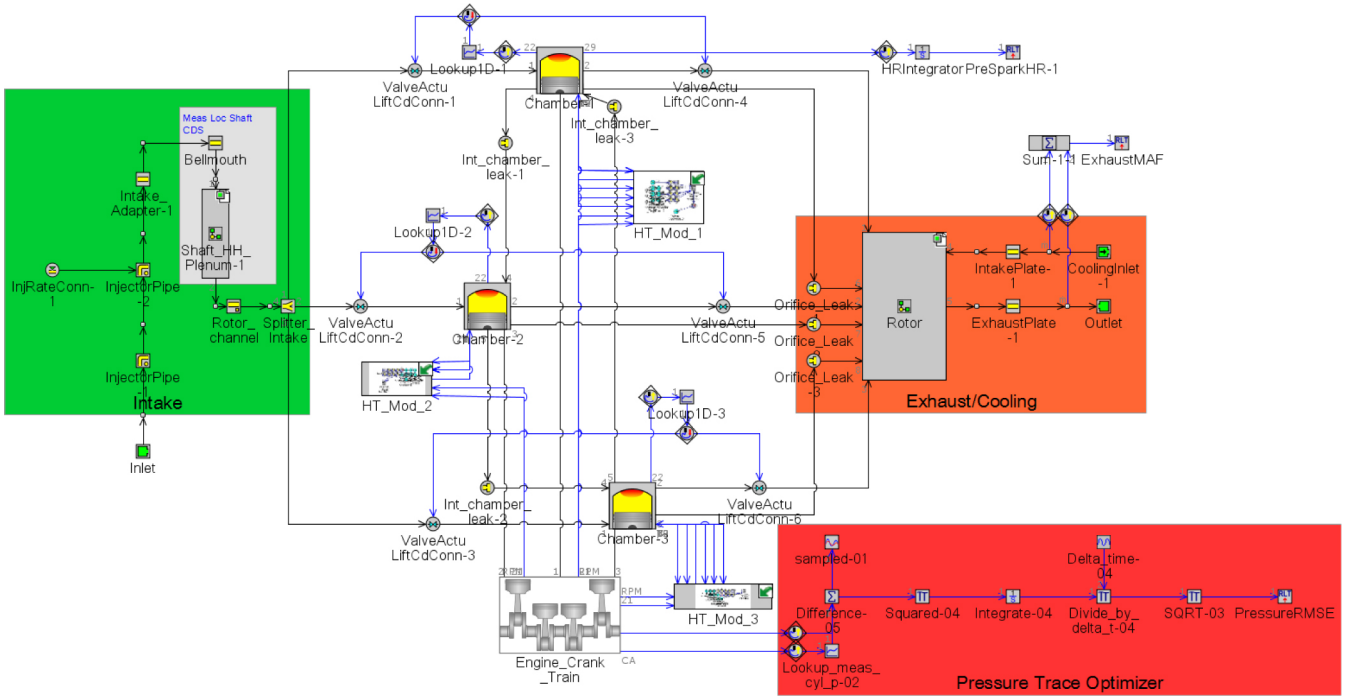

Figure 9. XMv3 GT-POWER model schematic.

By using input boundary conditions from the GT-POWER model, the surface model was simplified (Figure 10) to decrease the total number of cells in the domain, reducing computational cost. Since the objective of the presented work was to model combustion and heat transfer to the combustion chamber walls, upstream intake and exhaust path flow and rotor cooling flows were omitted.

An inflow boundary (from GT-POWER) was placed at the entrance to the rotor intake channel, greatly reducing the intake path volume while maintaining the same accuracy of the flow through the intake port. On the exhaust side, only the rotor segment attached to the exhaust port was modeled, and on both sides were positioned inflow and outflow boundary conditions (again from GT-POWER).

These simplifications allowed a boundary cell count reduction from 54 to 35, and domain cell count from 2 000 000 to 500 000 for the same base grid and mesh refinement settings.

Boundary Layer Modeling

The most popular approach to near-wall modelling in internal combustion engines (ICE) is to use logarithmic wall functions. These functions mitigate the need for extremely fine mesh to resolve flow profiles in a boundary layer, thus saving computational expense. In addition to boundary layer flow, logarithmic models also enable simplified calculations of heat flux in these regions. CONVERGE provides three “law of the wall” heat transfer models to select from. These are: the O’Rourke and Amsden model [20], the Han and Reitz model [10], and the Angelberger model [21].

To help select a model for XMv3 simulations, a comparison study was performed to investigate the effect of the wall heat transfer models on the calculated total heat losses. Simulation results and test data are depicted in Figure 11.

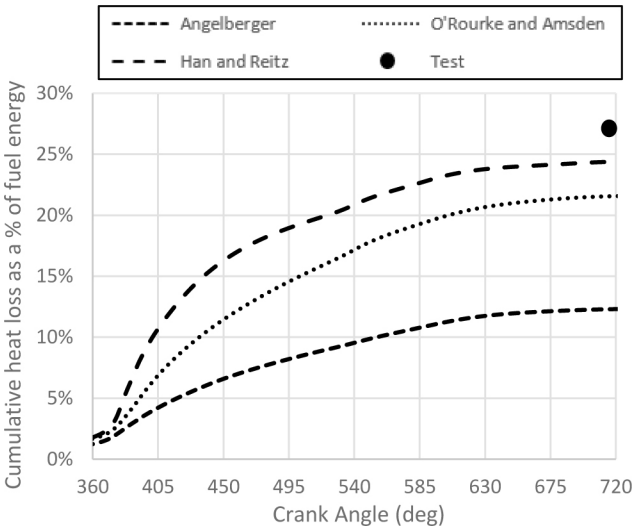

Figure 11. Comparison between experimental and calculated heat losses for various wall heat transfer models for case 1.

As shown by several authors [22] [23], wall heat transfer models that do not account for variable density effects in thermal boundary layer will under predict heat transfer. The Han and Reitz model is the only model available in CONVERGE that considers density variation, and it was also closest to the experimental results obtained in case 1 (as seen in Figure 11), so it was selected. Park [22] showed that this model in some part adopts partial variable density effects, and in other parts adopts assumptions of incompressible flows. Thus, full variable density effects on thermal boundary layers are not employed uniformly. In conclusion, the simplified representation of the boundary layer processes inherent to the law of the wall heat transfer models is possibly the reason why heat transfer losses are still slightly under-predicted by CFD.

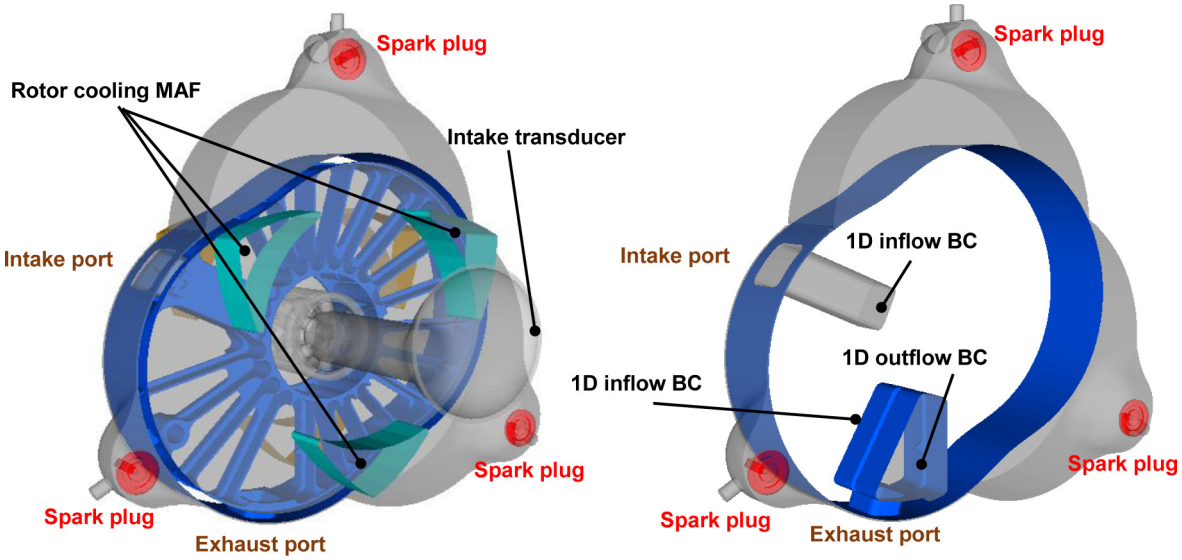

Figure 10. Computational domain used for the CONVERGE simulations using the full engine and boundary conditions from test (left), and from the simplified engine model using GT-POWER (right)

Grid Settings

Mesh grid settings are dependent on the physics to be resolved and on the computational costs to be tolerated. A grid independence study was performed for the XMv3 model, and Figure 12 shows the final cell sizes used to model general flow, spark ignition, and flame propagation. Adaptive mesh refinement (AMR) was used to automatically refine the grid based on fluctuating and moving conditions such as temperature and velocity. This technique refines the mesh only where necessary, avoiding a globally refined mesh or greater user expertise in defining an accurate variable mesh.

To specify a maximum level of refinement, a grid scale number (integer) is specified for each condition in which AMR is applied. CONVERGE then calculates the maximum grid refinement from the base grid as Equation 1 shows [24].

$$scaled\ grid = \frac{dx\_base}{2^{grid\_scale}} \quad (1)$$

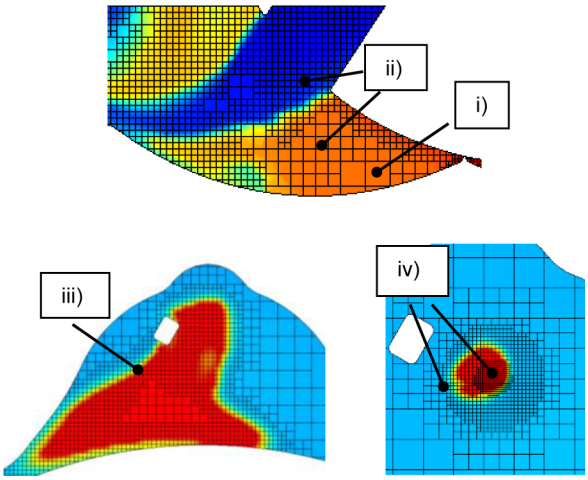

Figure 12. i) Base mesh size: 2.7 mm; ii) Velocity gradients were resolved by using velocity AMR in the intake channel and combustion chamber; iii) Temperature and species gradients were resolved for accurate flame propagation speed predictions.; iv) The grid in the vicinity of the spark plug was refined to resolve turbulence and ignition of the mixture with 0.08 mm to 0.17 mm cell sizes;

Near Wall Treatment

As previously mentioned, "Law of the Wall" models can estimate local velocities in the boundary layer without resolving the viscous sublayer. This method is computationally cheaper than resolving the flow at the viscous sublayer which requires very small y+ values. Y+ values relate the cell size adjacent to the wall to the physical location in the boundary layer based on the local velocity. Law of the wall heat transfer models have the highest errors when y+ is near to the linear-to-log transition point. This is also called the critical y+. When using wall models, it is recommended that y+ be maintained between 30 and 300 throughout the complete cycle simulation.

The AMR y+ capability available in CONVERGE allows an easy way to maintain the y+ values within the recommended range. If the absolute value of y+ in a cell exceeds the user specified number (300 in this case), the cell can be automatically embedded, thus reducing y+. A post simulation visualization of y+ values (using ENSIGHT software) is always performed to ensure compliance.

Spark Modelling

Spark energy discharge across the electrode gap was specified in CONVERGE as two energy sources, a breakdown phase and an arc/glow phase. As described by Heywood [14], fluid motion in the spark region is quite significant, therefore the arc between the electrodes is normally advected with the flow and stretches out in length. CONVERGE allows specification of the source as a moving line (a collection of 17 point sources) with flow between the electrode gap.

CALCULATION PROCEDURE AND RESULTS

A close match between measured and calculated chamber pressures vs. crankshaft angle (CA) is the best indicator of the accuracy of the 1D and CFD models, and there are four primary parameters adjusted to minimize error. These are: the volume vs. CA profile, the heat release rate, the heat transfer rate, and the gas leak mass flow rates (blow-by). The blow-by flows are represented and adjusted in the 1D model as equivalent critical orifice areas.

The heat transfer losses in the XMv3 engine were calculated using a combination of experimental, 1D, and CFD data. The iterative calculation method is presented in Figure 13.

Both motoring and firing experimental chamber pressure traces and intake MAF data were used for 1D model calibration. Beginning with motoring, the model's volume profile vs. CA (due to seal motion) and leakage areas were optimized to minimize deviation from experimental data across all engine speeds. Then, with these "motoring" parameters now fixed, firing trace comparisons were performed, adjusting heat release curves and heat transfer coefficients as needed to fit experimental data. The process was an iterative loop, as adjusting the heat transfer during firing would slightly affect the motoring traces, thus altering the required leak areas, thus altering the heat released on the firing cycle, etc. Since the "target" total heat transfer value was unknown at this point, a reasonable starting value of twice the experimentally measured heat transfer to the stationary parts was chosen. This assumed that half of the heat went into the rotor, and the other half into the stationary parts. The important end result of the 1D model work was not the value of heat transfer, but rather a set of boundary conditions for the CFD model, namely the mass flow rates and temperatures of all engine's flows. The CFD model was then used to generate an updated total heat transfer value, which was then fed back to the GT Power simulations, and the process repeated to adequate convergence.

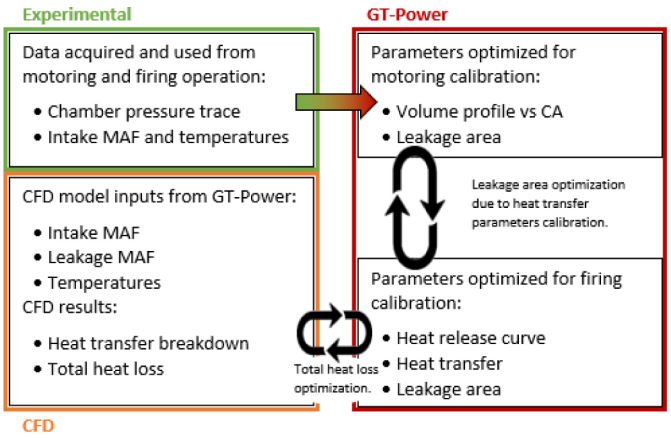

Figure 13. Flow chart of the calculation and matching process

Previous work from ARGONNE National Laboratory in collaboration with Convergent Science Inc. showed that SI CFD results contain cycle to cycle variability, just as in SI experiments [25]. Therefore, multi-cycle simulations with 5 to 6 consecutive cycles were run for each tested condition. The first cycle was never used because it could be subject to greater error from initial conditions, such as the faulty assumption of uniform spatial variations in flow conditions. The cycle that best fits the experimental (average of 50) and GT-POWER (not subject to variation) pressure traces was then selected for further analysis of heat transfer.

Again, if the total heat transfer values resulting from the CFD largely disagreed with the "target" used in GT-POWER, then the above mentioned procedure could be iterated, thus providing a more precise answer.

Figure 14 shows results from engine operation at 9000 rpm and full load. As it can be seen, both calculated pressures from GT-POWER and CFD closely follow experimentally measured pressure.

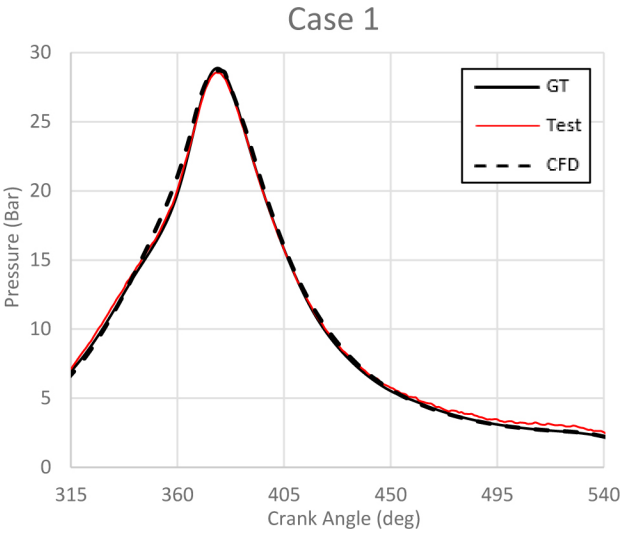

Figure 14. Comparison of pressure traces obtained experimentally, through GT-POWER and CONVERGE CFD for Case 1 (9000 rpm).

In order to calculate the total heat loss from experimental results, a derivative ratio between rotor and stationary parts heat transfer was taken from this CFD result, with the added assumption that thermal energy generated from friction goes only to the stationary parts. Table 4 shows the experimental and predicted heat transfer results for the 9000 rpm WOT "Cold Steady State" result.

Table 4. Experimental and model heat transfer results for case 1 - 9000 rpm, full load. All heat transfer losses are presented as a % of the fuel energy supplied.

	Stationary parts	Rotor
Measured heat loss	17%	-
Predicted heat loss	15%	9%
Predicted ratio between rotor and stationary parts	60%	
Predicted total heat losses (only from CFD / from experimental using the predicted ratio)	24% / 27%	

Experimental results indicate that 17% of fuel energy is lost to the stationary parts against 15% as predicted by CFD. CFD predicted 9% of energy lost to the rotor, with no experimental value available as comparison. Finally, a total energy loss of 24% of total fuel energy was predicted by CONVERGE, slightly under predicting the 27% measured experimentally based on the predicted 60% ratio between the rotor and stationary parts heat losses.

Results for 5000 rpm at full load, also "Cold Steady State", are presented in Figure 15. In this case, the peak pressure was accurately predicted by CFD, with start of combustion and expansion stroke showing slightly higher pressure figures than experimental / GT-POWER. Additional CFD cycles could be run until a better match was found, but these results were deemed satisfactory for the purposes of the present work.

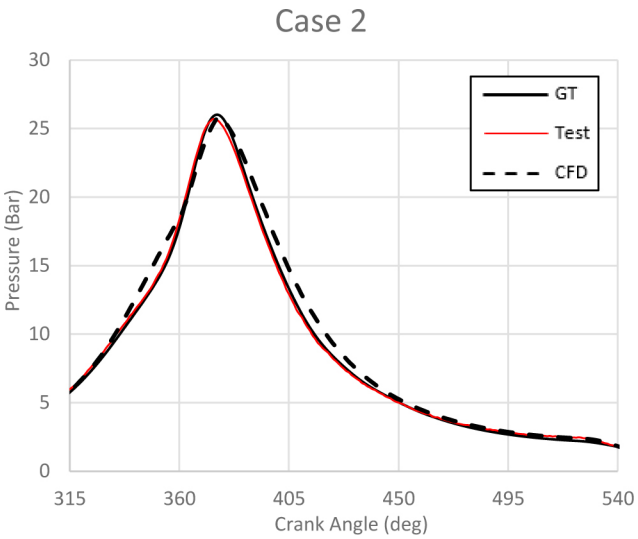

Figure 15. Comparison of pressure traces obtained experimentally, through GT-POWER and CONVERGE CFD for Case 2 (5000 rpm).

As expected, calculated and measured heat losses for case 2 are higher than those obtained for case 1 because of the reduced engine speed. However, CFD predicts nearly the same ratio (60%) between the stationary parts and rotor heat losses (Table 5).

Table 5. Experimental and model heat transfer results for case 2 - 5000 rpm, full load. All heat transfer losses are presented as a % of the fuel energy supplied.

	Stationary parts	Rotor
Measured heat loss	22%	-
Predicted heat loss	21%	12%
Predicted ratio between rotor and stationary parts	60%	
Predicted total heat losses (only from CFD / from experimental using the predicted ratio)	34% / 33%	

The results described were specific to one engine test, and other tests showed different heat losses (between 18% and 35% at 5000 rpm, full load). For example, another heat transfer data point was collected during durability testing. The engine ran for 6.5 hours at 5000 rpm, full load, and the total heat transfer losses as a function of test time is shown below in Figure 16. In this test, the cooling flow was 97 kg/h for the housing and 67 kg/h for the rotor, with lambda of 0.7, thus representing a more typical warmer operating condition of the engine with lower cooling flows than Case 1 and Case 2 presented above.

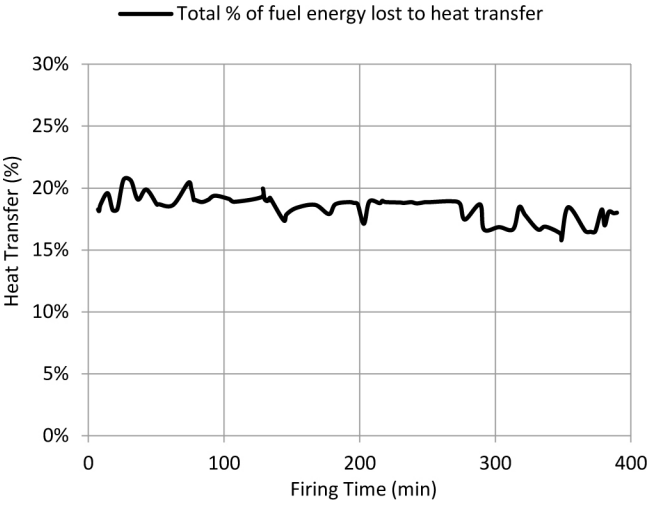

Figure 16. Total heat transfer results during 6.5 hour durability test.

The average heat transfer loss during this test was ~18%. Because the engine is still under development, it remains highly sensitive to changes in hardware such as the changes of seal type, seal condition/ blow-by amount, metal coatings, etc, as well as changes in operating conditions, including cooling flow rates, air-fuel ratio, and spark timing. Of course, all these factors affect heat transfer.

Heat transfer losses in the XMv3 engine in these three tests were shown to range from 18% up to 35% of fuel energy, and a peak indicated efficiency of 22% was achieved. Further work remains to be done to match heat transfer cases other than the one shown in Table 4 or Table 5. The XMv3 heat transfer results are in line with or lower than those of conventional small scale piston engines with similar compression ratios [14].

CONCLUSION AND FUTURE WORK

A combined method to measure and predict heat transfer losses on the LiquidPiston's XMv3 engine was presented. The method used a GT-POWER model, calibrated with experimental results, which supplied boundary conditions to a CONVERGE CFD model. The models were iterated as required to achieve acceptable levels of error.

Due to the fact that rotor cooling air inevitably mixes with exhaust gases of the engine, it was not possible to directly measure the energy lost to the rotor. Therefore, the CFD results were used to calculate a derivative ratio between the energy transferred to the engine stationary parts vs. the moving rotor. CFD results showed that the heat transferred to the rotor was 60% of that to the stationary parts for both of the engine speeds tested. Estimated overall heat losses varied from 18% to 34% of the fuel energy for the 5000 rpm case and 27% for the 9000 rpm case each at full load. The CFD predictions were close to some of the experimental measurements, particularly those with especially high cooling flows. Further experimental and analytical work remains to be done to obtain a match for all test cases.

Consistent experimental measurements were challenging. They were likely sensitive to confounded variables such as seal type, seal condition/blow-by, and coatings used.

The predictive models developed will inform future engine cooling system optimization work, leading to higher power densities and thermal efficiencies. Current results are already market competitive in the 3 horsepower size.

Future work intends to use a more accurate procedure for heat transfer loss measurement, by using a surface temperature thermocouple [26] allowing for direct heat flux calculation from the in-cylinder gases to the chamber walls. In this way, calculated heat flux curves can be directly compared with experiments and a better validation of the models can be performed. Furthermore, the previous simplification assumption of a constant rotor surface temperature will be eliminated in order to minimize calculation errors in rotor heat flux. For this purpose, CONVERGE Conjugate Heat Transfer (CHT) capability will be used to predict rotor metal temperature. Under these conditions, the flow and heat transfer will be solved simultaneously in both the solid and fluid regions. In this way, flow and heat transfer can be modelled on both sides of the rotor, i.e. combustion chamber and rotor cooling, to predict the local rotor surface temperature facing the combustion chamber. This will allow for a more accurate calculation of the heat flux.

REFERENCES

1. Sprague S. B., Park S., Walther D. C., Pisano A. P., and Fernandez-pello A. C., “Development and characterisation of small-scale rotary engines,” *Int. J. Altern. Propuls.*, vol. 1, no. 2/3, pp. 275-293, 2007.
2. Froede, W., "The NSU-Wankel Rotating Combustion Engine," SAE Technical Paper 610017, 1961, doi:10.4271/610017.
3. Shkolnik A. and Shkolnik N., “High Efficiency Hybrid Cycle (HEHC) Thermodynamic Cycle,” US Patent 8,365,698, 2007.
4. Ribeiro, B. and Martins, J., "Direct Comparison of an Engine Working under Otto, Miller and Diesel Cycles: Thermodynamic Analysis and Real Engine Performance," SAE Technical Paper 2007-01-0261, 2007, doi:10.4271/2007-01-0261.
5. Martins, J., Uzuneanu, K., Ribeiro, B., and Jasasky, O., "Thermodynamic Analysis of an Over-Expanded Engine," SAE Technical Paper 2004-01-0617, 2004, doi:10.4271/2004-01-0617.
6. Torregrosa J., Olmeda P. C., and Romero C. A., “Revising Engine Heat Transfer,” *J. Eng. Ann. Fac. Eng. Hunedoara*, no. 3, pp. 245-265, 2008.
7. Woschni, G., "A Universally Applicable Equation for the Instantaneous Heat Transfer Coefficient in the Internal Combustion Engine," SAE Technical Paper 670931, 1967, doi:10.4271/670931.
8. Gorla R. and Bartrand T., “Couette flow heat loss model for the rotary combustion engine,” *Proc. Inst. Mech. Eng.*, vol. 6, no. 210, p. 587, 1996.
9. Rakopoulos C., Kosmadakis G., and Pariotis E., “Critical evaluation of current heat transfer models used in CFD in-cylinder engine simulations and establishment of a comprehensive wall-function formulation,” *Appl. Energy*, vol. 87, no. 5, pp. 1612-1630, 2010.
10. HAN Z. and Reitz R., “A Temperature Wall Function Formulation for Variable-density Turbulent Flows with Application to Engine Convective Heat Transfer Modeling,” *Int. J. Heat Mass Transf.*, vol. 40, no. 3, pp. 613-625, 1997.
11. Wimmer, A., Pivec, R., and Sams, T., "Heat Transfer to the Combustion Chamber and Port Walls of IC Engines -Measurement and Prediction," SAE Technical Paper 2000-01-0568, 2000, doi:10.4271/2000-01-0568.
12. Ebrahimi K. M., Lewalski A., Pezouvanis A., and Mason B., “Piston Data Telemetry in Internal Combustion Engines,” *Am. J. Sens. Technol.*, vol. 2, no. 1, pp. 7-12, 2014.
13. Badgley P., Kamo R., and Doup D., “Adiabatic Wankel Type Rotary Engine,” 1988.
14. Heywood J., *Internal Combustion Engine Fundamentals*. McGraw-Hill, Inc., 1988.
15. Meng P., Rice W., Schock H., and Pringle D., “Preliminary Results on Performance Testing of a Turbocharged Rotary Combustion Engine,” 1982.
16. Shkolnik, A., Littera, D., Nickerson, M., Shkolnik, N. et al., "Development of a Small Rotary SI/CI Combustion Engine," SAE Technical Paper 2014-32-0104, 2014, doi:10.4271/2014-32-0104.
17. Littera D., Nickerson M., Kopache A., Machamada G., Sun C., Schramm A., Medeiros N., Becker K., Shkolnik S., and Shkolnik A., “Development of the XMv3 High Efficiency Cycloidal Engine,” SAE Technical Paper 2015-32-0719, 2015.
18. Munson B., YOUNG D., OKIISHI T., and HUEBSCH W., *Fundamentals of Fluid Mechanics*, Sixth Edit. Don Fowley, 2009.
19. Science C., “Converge CFD software.” [Online]. Available: https://convergecfd.com/. [Accessed: 19-Jan-2016].
20. Amsden A., “KIVA-3V: A Block Structured KIVA Program for Engines with Vertical or Canted Valves,” 1997.
21. Angelberger, C., Poinsot, T., and Delhay, B., "Improving Near-Wall Combustion and Wall Heat Transfer Modeling in SI Engine Computations," SAE Technical Paper 972881, 1997, doi:10.4271/972881.
22. Park H. J., “DEVELOPMENT OF AN IN-CYLINDER HEAT TRANSFER MODEL WITH VARIABLE DENSITY EFFECTS ON THERMAL BOUNDARY LAYERS,” The university of the Michigan, 2009.
23. Nijeweme D., Kok J., Stone C., and Wyszynski L., “Unsteady in-cylinder heat transfer in a spark ignition engine : experiments and modelling,” *Proc. Inst. Mech. Eng. Part D J. Automob. Eng.*, vol. 215, 2001.
24. C. S. Inc., Ed., *CONVERGE 2.2 Theory Manual*. 2015.
25. Scarcelli, R., Richards, K., Pomraning, E., Senecal, P. et al., "Cycle-to-Cycle Variations in Multi-Cycle Engine RANS Simulations," SAE Technical Paper 2016-01-0593, 2016, doi:10.4271/2016-01-0593.
26. Fahl H., “The validation of the explosive fumes dynamics in rooms,” *New Trends Res. Energ. Mater.*, pp. 124-134, 2009.

CONTACT INFORMATION

Tiago Costa is a PhD student from the MIT-Portugal (LTI Program) at University of Minho. He can be reached at:

id5739@alunos.uminho.pt

ACKNOWLEDGMENTS

The authors wish to thank other members of the engineering / technical team which helped in the design and testing of the XMv3 engine, including especially: Alexander Kopache, Chuankai Sun, Ganapathy Machamada, Alex Schramm, Adarsh Ganesan, Alexei Sondergeld, Davis Parker, Ritwik Athalye, Jeremy Serini, Ryan Leary. We also would like to thank DARPA for their funding and support.

This research was developed with funding from the Defense Advanced Research Projects Agency (DARPA). The views, opinions, and/or findings expressed are those of the authors and should not be interpreted as representing the official views or policies of the Department of Defense or the U.S. Government.

The authors would like also to acknowledge the team at Convergent Science for the support given, and EnSight for the software license provided.

Tiago Costa benefits from the PhD grant PD/BD/l05929/2014, financed by National funds from the Ministry of Education and Science through FCT - Fundacao para a Ciencia e a Tecnologia. Francisco Brito benefits from the Post doctoral grant SFRH/BPD/89553/2012, financed by FEDER funds through Programa Operacional Fatores de Competitividade - COMPETE and National funds through PIDDAC and FCT - Fundacao para a Ciencia e a Tecnologia.

DEFINITIONS/ABBREVIATIONS

AMR - Adaptive mesh refinement

ATDC - After Top Dead Center

BTDC - Before Top Dead Center

CA - Crankshaft Angle

CAD - Computer Aided Design

CFD - Computer Fluid Dynamics

CFL - Courant Friedrich Lewy

CHT - Conjugate Heat Transfer

CR - Compression Ratio

EPO - Exhaust Port Close

HEHC - High Efficiency Hybrid Cycle

ICE - Internal Combustion Engine

IPC - Intake Port Close

MAF - Mass Air Flow

RANS - Reynolds-average Navier-Stokes

RNG - Renormalization group

SA - Spark Advance

SI - Spark Ignition

TDC - Top Dead Center

WOT - Wide open throttle